Int. J. Multiphase Flow Vol. 19, No. 6, pp. 965–986, 1993
Printed in Great Britain.

0301-9322/93 $6.00 + 0.00

NUCLEATION AND FLASHING IN NOZZLES—2

COMPARISON WITH EXPERIMENTS USING A FIVE-EQUATION MODEL FOR VAPOR VOID DEVELOPMENT

V. N. BLINKOV,[1] O. C. JONES[2]† and B. I. NIGMATULIN[3]

[1]Department of Engines, Thermal Physics Aviation Institute, Kharkov 310 070, Ukraine

[2]Department of Nuclear Engineering and Engineering Physics and Center for Multiphase Research, Rensselaer Polytechnic Institute, Troy, NY, U.S.A.

[3]N.P.O. Energia, Moscow, Russia

(Received 20 December 1990; in revised form 12 August 1993)

Abstract—A quasi-one-dimensional, five-equation, homogeneous, nonequilibrium model has been developed and utilized on a microcomputer to calculate the behavior of flowing, initially subcooled, flashing water systems. Equations for mixture and vapor mass conservation, mixture momentum conservation, liquid energy conservation and bubble transport were discretized and linearized semi-implicitly, and solved using a successive iteration Newton method. Closure was obtained through simple constitutive equations for friction and spherical bubble growth, and a new nucleation model for wall nucleation in small nozzles combined with an existing model for bulk nucleation in large geometries to obtain the thermal nonequilibrium between phases. The model described was applied to choked nozzle flow with subcooled water inlets based on specified inlet conditions of pressure and temperature, and vanishing inlet void fraction and bubble number density. Good qualitative and quantitative agreement with the experiment confirms the adequacy of the nucleation models in determining both the initial size and number density of nuclei, and indicates that mechanical nonequilibrium between phases is not an important factor in these flows. It is shown that bulk nucleation becomes important as the volume-to-surface ratio of the geometry is increased.

Key Words: critical flow, nucleation, bubble growth, bubble number density, cavities, vapor generation, interfacial area

1. INTRODUCTION

The first paper in this sequence (Shin & Jones 1993, this issue, pp. 943–964) described the technology relative to the initiation or inception of the flashing phenomena and showed the development of a model for nucleation from the walls in pipes and nozzles. This model was utilized to describe the development of the bubble population and the resultant onset of thermal nonequilibrium between the phases in such situations. The model provided a method of predicting the superheat which develops and, for the first time, provides a link between the microscopic description of wall-cavity-based nucleation and bubble growth, and the macroscopic global flow parameters.

When the new model was applied to flashing flows in nozzles, it was shown that negligible voids developed upstream of the throat, even in the most energetic of cases where throat superheats approached 100 K. Predictions developed from the model of superheat at the flashing inception point‡ were within 2 K, and resultant confirmatory calculations of critical discharge rates within 3%.

First principles calculated of void development requires both the superheat and area density for phase transformation, the latter requiring both the number and size of the bubbles. The new nucleation model provides this information. It is the purpose of this paper to provide a rational framework for the computation of void development downstream of the inception location in pipes, nozzles and restrictions. Further, it will be shown that excellent agreement is obtained between calculated and experimental results confirming that, while slip is not an important factor in critical

†Author for correspondence.

‡The point of flashing inception is considered to be equivalent to the "point of net vapor generation (NVG)" in boiling. For nozzles, this point is taken to be the throat.

and near-critical, low-quality flow conditions, thermal nonequilibrium can be an overriding factor in obtaining predictive accuracy.

The general framework used in the numerical development is not particularly new except for some specific details which will be delineated in the development. Rather, what is, perhaps, new in addition to the new description of thermal nonequilibrium development, is the use of such a detailed numerical model on a personal computer, in this case a Hewlett-Packard model 9816. This machine is based on the 32-bit MC-68000 microprocessor so can be considered the forerunner of more modern 32-bit machines. As such, the use of such methods on the newer and faster 80386 microprocessor running at 16–24 MHz should be considerably faster than the experience reported herein. The practicality of such computational frameworks on "desk-top" computers thus appears to be within reach.

2. DEVELOPMENT

Flow Regimes

Among the variety of internal two-phase flow structures, the bubble, slug, churn, annular, dispersed–annular and dispersed regimes have been identified. These classifications and their respective transition criteria both have a qualitative nature, so models constructed with the use of these flow maps may utilize existing transition criteria for comparison with data. Advanced, best-estimate computer programs for transient analysis of two-phase systems, such as TRAC (LASL 1979) and RELAP (Chow & Ransom 1984), apply flow regime maps with void fraction, ϵ, as the main transition criterion. Indeed, while other methods exist which are more detailed and which are, perhaps, more accurate for specific transitions, the use of void fraction has achieved wide recommended general usage due to its simplicity (Wu *et al.* 1981; Ishii & Mashima 1983). In what follows, two variants of this flow structure scheme are considered. A comparison of the resultant features of these two maps will be discussed following identification of the given equations particular to the two situations.

Flow regime 1 [figure 1(a)]

Flashing inception is assumed to result in a bubbly mixture. The limits of this regime vary depending on the rate of void development. For slowly developing systems, the transition is generally taken to be at approximately $\epsilon \cong 0.2$. For rapidly expanding systems, the transition to slug or churn flows may be inhibited until quite large void fractions up to >0.7 are obtained. For the purpose of this discussion the bubbly mixture is assumed to exist up to $\epsilon = 0.3$, consistent with previous assumptions (Wu *et al.* 1981; Dobran 1985). Note that Ishii & Mashima (1983) showed that for $\epsilon > 0.3$ spherical bubbles must touch. For bubbly flows to exist at larger void fractions, obviously the bubbles must distort. Such is the case observed in liquid-metal MHD generators. In

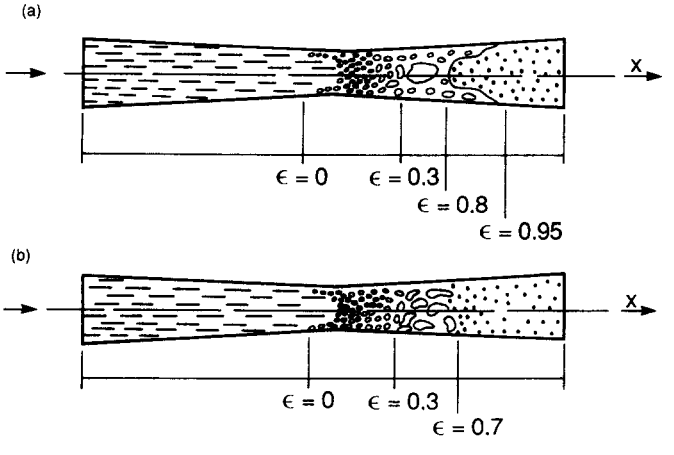

Figure 1. Assumed flow diagrams of flashing liquid in nozzles: (a) flow regime map 1; (b) flow regime map 2.

moderately accelerating systems, agglomeration begins to occur after bubbles begin to touch, thus leading to transition of the bubbly structure to the adjacent regime.

As void development continues past $\epsilon > 0.3$, it is assumed that this coalescence results in the formation of larger bubbles with the region between filled with small bubbles. This bubbly–slug regime is taken to exist throughout the region $0.3 < \epsilon < 0.8$, whereupon the slugs have grown so long that they, in turn, coalesce to form annular flow or mist–annular. Dispersed droplet flow is assumed to exist for void fractions >0.9. The region between $\epsilon = 0.8$ and 0.95 is considered herein to be transitional zone coupling slug and dispersed liquid flows.

Flow regime 2 [figure 1(b)]

In this case, the structure of slug flow is not developed and the zone between $\epsilon = 0.3$ and 0.7 is considered as a transitional zone. This zone may be characterized by intensive interaction or coalescence of bubbles and deviations from sphericity, characteristic of the churn–turbulent regime (Solbrig *et al.* 1978). In this case, dispersed flow is assumed to occur as a breakdown of the continuous liquid filaments resulting in continuous vapor dispersed flows.

Two-phase Flow Model

For the current case the interest is in the lower void fraction regions below dispersed flows. In such cases, the vapor is tightly coupled to the liquid from a mechanical viewpoint, relative velocities are small and variations are due more to distribution than local slip. It is thus assumed that mechanical equilibrium exists and the phases have identical velocities and pressures. Vapor temperatures are assumed to be at local saturation conditions, since the primary source of heat transfer is through the liquid continuum which may be subcooled, saturated or superheated locally (according to the local pressure).

The model thus chosen is a quasi-one-dimensional, transient model which uses two continuity equations (mixture and vapor phase), one energy equation for the liquid, one momentum equation for the mixture and one bubble transport equation. These are expressed below:

continuity equation for the mixture

$$\frac{\partial \varrho_M}{\partial t} + \frac{1}{A}\frac{\partial}{\partial z}(\varrho_M A w) = 0; \qquad [1]$$

continuity equation for the vapor phase,

$$\frac{\partial \epsilon \varrho_V}{\partial t} + \frac{1}{A}\frac{\partial}{\partial z}(\epsilon \varrho_V A w) = \Gamma_V; \qquad [2]$$

momentum equation for the mixture,

$$\frac{\partial w}{\partial t} + w\frac{\partial w}{\partial z} = -\frac{1}{\varrho_M}\frac{\partial p}{\partial z} - \frac{1}{\varrho_M} f_f; \qquad [3]$$

energy equation for the liquid,

$$\frac{\partial}{\partial t}[(1-\epsilon)\varrho_L u_L] + \frac{1}{A}\frac{\partial}{\partial z}[(1-\epsilon)\varrho_L u_L A w] + \frac{p}{A}\frac{\partial}{\partial z}[(1-\epsilon)A w] = p\frac{\partial \epsilon}{\partial t} - \Gamma_V i_f - A_i q''_{i,net}; \qquad [4]$$

and

conservation of bubble number density,

$$\frac{\partial N_B}{\partial t} + \frac{1}{A}\frac{\partial}{\partial z}(N_B A w) = J_w + J_B. \qquad [5]$$

Note in these equations that t is time, w is taken as the z-direction velocity, and ϱ is density, in general with the subscripts M, L and V representing mixture, liquid and vapor respectively, phases not necessarily at saturation, and the subscripts F and G representing saturated liquid and vapor. Also, A is the cross-sectional duct area, Γ_V is the volumetric rate of vapor generation, p is the pressure, f_f is the volumetric friction force (friction force per unit volume), D is the duct diameter or hydraulic diameter, u is the specific internal energy, ϵ is the void fraction, i is the

enthalpy with the same subscript definitions as for density, $q''_{i,net}$ is the net interfacial heat flux, A_i is the interfacial area density, N_B is the number density of the bubbles and J is the volumetric equivalent nucleation rate with the subscripts w and B representing wall and bulk, respectively. It is assumed that there is no slip. This is in accordance with the intention that this model be utilized to predict void development in critical or near-critical flows of high velocity where relative velocities are expected to be of negligible importance.

The unknowns in this equation set include the void fraction, ϵ, pressure, p, axial velocity, w, liquid temperature, T_L, and bubble number density, N_B, where T_L is tied to the specific internal energy u_L through the caloric equation of state.

Constitutive equations—flow regime map 1

The constitutive equations for wall friction and interfacial heat and mass transfer must be provided for closure as well as those for nucleation.

Wall friction. For single-phase flow ($\epsilon = 0$) the shear stress is taken to be

$$\tau_w = \tfrac{1}{2} C_f \varrho_L w^2, \tag{6}$$

where the friction coefficient is correlated with the liquid Reynolds number, Re_L, as

$$C_f = C_f(Re_L) \quad \text{with } Re_L = \frac{\varrho_L w D}{\mu_L}. \tag{7}$$

The Blasius friction coefficient C_f is used for turbulent flow and μ is viscosity, with the same subscripts as for other properties. The wall friction force per unit volume of the mixture is

$$f_f = \tau_w \frac{\xi \, dz}{A \, dz} = 2C_f \frac{\varrho_L w^2}{D}, \tag{8}$$

the duct perimeter is ξ. For two-phase flow, a friction multiplier, ϕ^2, is utilized so that

$$f_f = 2C_f \phi^2 \frac{\varrho_M^2 w^2}{\varrho_L D}, \tag{9}$$

where the friction coefficient and Reynolds number relationships are given by [7]. The multipliers used were taken from Beattie (1973) as included in RETRAN (McFadden *et al.* 1981), where a flow regime map similar to that utilized herein was used. The two-phase friction multiplier equations adopted in terms of the quality, x, are:

for $\epsilon < 0.3$,

$$\phi^2 = \left[1 + x\left(\frac{\varrho_L}{\varrho_V} - 1\right)\right]^{0.8} \left\{1 + x\left[\frac{(3.5\mu_V + 2\mu_L)\varrho_L}{(\mu_V + \mu_L)\varrho_V} - 1\right]\right\}^{0.2}; \tag{10}$$

for $0.3 \leqslant \epsilon < 0.8$,

$$\phi^2 = \left[1 + x\left(\frac{\varrho_L}{\varrho_V} - 1\right)\right]^{0.8} \left[1 + x\left(3.5\frac{\varrho_L}{\varrho_V} - 1\right)\right]^{0.2}; \tag{11}$$

for $0.8 \leqslant \epsilon < 0.95$,

$$\phi^2 = \left[1 + x\left(\frac{\varrho_L}{\varrho_V} - 1\right)\right]^{0.8} \left[1 + x\left(\frac{\mu_V \varrho_L}{\mu_L \varrho_V} - 1\right)\right]^{0.2}; \tag{12}$$

and

for $\epsilon > 0.95$,

$$\phi^2 = \left(\frac{\mu_V}{\mu_L}\right)^{0.2} \left(\frac{\varrho_V}{\varrho_L}\right)^{0.8} \left[1 + x\left(\frac{\varrho_L}{\varrho_V} - 1\right)\right]^{1.8}. \tag{13}$$

Interfacial heat and mass transfer. The rate of vapor generation is limited by the heat transfer rate and interfacial area according to the relation

$$\Gamma_V = \frac{A_i \dot{q}''_{i,net}}{\Delta i_{FG}}, \tag{14}$$

where

$$\dot{q}''_{i,net} \equiv \frac{1}{A_i}\int_{A_i}\sum_{k=L,V}\dot{\mathbf{q}}''_k \cdot \mathbf{n}_k \, dA_i, \qquad [15]$$

where $\mathbf{q}''_k$ is the heat flux for phase k and $\mathbf{n}_k$ is the unit outward normal to phase k. Relationship [14] shows that evaporation is due to energy absorbed or released at the interface in the form of latent heat of phase change.

(a) For bubbly flow, $\epsilon < 0.3$, the model assumes that the zone of intensive nucleation is very narrow, $L_{nuc} \ll L$, where L is the nozzle inlet length, and is located very close to the minimum area portion of the nozzle. This has been confirmed by calculations and is consistent with the distributed nucleation model presented in the companion paper (Shin & Jones 1993). In this case, uniformly sized bubbles may be assumed to exist at any cross section. From sphericity, the interfacial area density A_i is given by

$$A_i = 4\pi R_B^2 N_B, \qquad [16]$$

where N_B is the bubble number density and R_B is the bubble radius. Also,

$$\epsilon = \tfrac{4}{3}\pi R_B^3 N_B = \tfrac{1}{3} A_i R_B \qquad [17]$$

so that

$$A_i = (36\pi N_B)^{1/3}\epsilon^{2/3} = \frac{3\epsilon}{R_B}. \qquad [18]$$

The growth of the bubbles is assumed to be controlled by transient conduction. An analytical solution of thermally-controlled bubble growth for constant values of liquid superheat due to Scriven (1959), expressed by an approximation given by Labuntzov *et al.* (1964), gives the heat input from the liquid to the bubble–liquid interface as

$$\dot{q}''_{i,net} = h\Delta T_{sup}, \qquad [19]$$

where the heat transfer coefficient is given by

$$h = \frac{k_L \mathrm{Nu}}{2R_B} \qquad [20]$$

with the Nusselt number expressed in terms of the Jakob number as

$$\mathrm{Nu} = \frac{12}{\pi}\mathrm{Ja}\left[1 + \frac{1}{2}\left(\frac{\pi}{6\mathrm{Ja}}\right)^{2/3} + \frac{\pi}{6\mathrm{Ja}}\right]. \qquad [21]$$

The Jakob number is defined as

$$\mathrm{Ja} \equiv \frac{C_{pL}\varrho_L(T_L - T_{sat})}{\varrho_V \Delta i_{FG}} = \frac{C_{pL}\varrho_L \Delta T_{sup}}{\varrho_V \Delta i_{FG}}. \qquad [22]$$

In this case, C_{pL} is the specific heat of the liquid and T is the temperature with subscripts L and V representing liquid and vapor, respectively, and the subscript sat indicating saturation. Similarly, ΔT_{sup} is the liquid superheat and Δi_{FG} is the latent heat. While [21], in general, is valid only for uniform superheat and not for variable pressure fields (Jones & Zuber 1978), it has been shown to be approximately correct when the *local* superheat is used (Wu *et al.* 1981).

(b) For bubbly–slug flow in the range $0.3 < \epsilon < 0.8$ it is assumed that some of the bubbles coalesce to form larger (Taylor) bubbles, while others continue to grow according to [19]–[22]. Thus, two classes of bubbles are assumed to exist and grow at different rates.

Since vapor generation may take place on the surface of both kinds of bubbles, the total interfacial flux is given by

$$\dot{q}''_{i,net} = \dot{q}''_S A_S + \dot{q}''_B A_B, \qquad [23]$$

which is the sum of the net heat flux going into evaporation along the slugs plus that for the small,

spherical bubbles. The subscripts for heat flux are S for Taylor-like bubbles and B for small, spherical bubbles which have not yet agglomerated. The Taylor bubbles are assumed to be cylinders which, at $\epsilon = 0.8$ absorb all smaller bubbles and merge with one another to form annular flow (Wu *et al.* 1981). The interfacial area density is thus given by

$$A_i = A_{iS} + A_{iB}, \quad [24]$$

where again the subscripts represent Taylor bubbles and spherical bubbles. For the Taylor bubbles the area density is

$$A_{iS} = \frac{4\epsilon^{2/3}}{\epsilon_{S_{max}}^{1/6} D} \quad [25]$$

and for the spherical bubbles left in the slugs it is given by

$$A_{iB} = \frac{3\epsilon_B}{R_B}. \quad [26]$$

Note that the total void fraction is the sum of that due separately to the slugs and the bubbles:

$$\epsilon = \epsilon_S + \epsilon_B. \quad [27]$$

The void fraction for the Taylor-like bubbles is given by the relation

$$\epsilon_S = \frac{1}{1 - \epsilon_{B_{max}}} \left\{ \epsilon - \epsilon_{B_{max}} \left[1 - \frac{(\epsilon - \epsilon_{B_{max}})(1 - \epsilon_{S_{max}})}{\epsilon_{S_{max}} - \epsilon_{B_{max}}} \right] \right\}, \quad [28]$$

where $\epsilon_{B_{max}} = 0.3$ and $\epsilon_{S_{max}} = 0.8$. The heat transfer coefficient appropriate for Taylor bubbles is approximated by that given in the TRAC-P1A code (LASL 1979) for slug flows correlated in terms of the Stanton number,

$$St_L \equiv \frac{Nu_L}{Re_L Pr_L} = 0.0073 \quad [29]$$

with Pr the Prandtl number. Thus, the interfacial heat transfer to the Taylor bubbles is

$$\dot{q}''_S = 0.0073 \varrho_L w C_{pL} (T_L - T_V). \quad [30]$$

(c) For the case of transitional and dispersed droplet flows where $\epsilon > 0.8$, the difference is in the friction multiplier as expressed in [10]–[13]. The heat and mass transfer occur on liquid droplets formed as a result of bubble coagulation and droplet entrainment from the lateral surface of the Taylor bubbles. In this case, the interfacial area density is given by

$$A_i = \frac{3(1 - \epsilon)}{R_d}, \quad [31]$$

where R_d is the droplet diameter. In this case, the net interfacial heat flux is

$$\dot{q}''_{i,net} = \frac{k_L Nu}{2R_d} (T_L - T_V). \quad [32]$$

In this case, the Nusselt number is assumed to be constant at a value of 16, as suggested by Solbrig *et al.* (1978). The droplet diameter is assumed to be

$$R_d = \frac{\sigma We}{2\varrho_V (w_V - w_L)^2}, \quad [33]$$

where the Weber number, We, is assumed to be constant at 5. Note that although no slip is considered in the conservation equations, droplet heat and mass transfer require a value for the relative velocity and this is calculated based on solid particle dynamics. A simple formulation which eliminates the transcendental nature of the drag–Reynolds number relationships was used (Jones

1984). The terminal Reynolds number for the droplets is taken as a function of the Archimedes number, Ar, as

$$\mathrm{Re} = \begin{cases} \dfrac{\mathrm{Ar}}{18}[1 + 0.0487(\frac{4}{3}\mathrm{Ar})^{0.452}]^{-1} & \mathrm{Ar} < 3.227 \times 10^5 \\ 1.74\sqrt{\mathrm{Ar}} & \begin{cases} \mathrm{Ar} \geqslant 3.227 \times 10^5 \\ \mathrm{Re} \leqslant 2 \times 10^5, \end{cases} \end{cases} \quad [34]$$

where

$$\mathrm{Ar} = \frac{f\varrho_L \Delta\varrho \delta^3}{\mu_L^2}. \quad [35]$$

The gravitational acceleration is g, the droplet diameter is δ and the positive liquid–vapor density difference is $\Delta\varrho$. The Reynolds number is based on the droplet diameter and the terminal velocity, taken to be the same as the relative velocity.

Constitutive equations—flow regime map 2

In bubbly flows there are no differences from flow regime map 1. The surface area density is proportional to $\epsilon^{2/3}$ assuming $N_B^{2/3}$ is constant. If the void fraction exceeds 0.3, the surface area density is influenced by two opposing effects. On the one hand, the continuing bubble growth and distortion of their shape tend to increase the area density, A_i. On the other hand, the coalescence and formation of large bubbles tends to reduce A_i. The variation of A_i with void fraction here may be small so it can be assumed that A_i remains constant having the value obtained at $\epsilon = 0.3$. The heat flux for bubbly flow is obtained from [19]–[22].

For the case where $\epsilon \geqslant 0.7$, the transition to dispersed droplet flow occurs and the interfacial area density is given by

$$A_i = \frac{3(1-\epsilon)}{R_d} = (36\pi N_d)^{1/3}(1-\epsilon)^{2/3}. \quad [36]$$

Thus, the variation with ϵ is assumed to be symmetrical about $\epsilon = 0.5$. Thus, $A_i \cong \epsilon^{2/3}$ if $\epsilon < 0.3$, and $A_i \cong (1-\epsilon)^{2/3}$ if $\epsilon > 0.7$. The Nusselt number for the heat flux is determined by [31]–[33].

Nucleation Kinetics

The overall flashing process is governed by nonequilibrium thermal conditions with superheated liquid and saturated vapor generally coexisting in the flow field. The initial superheat of the liquid is generated due to rate limitations on the phase change process during the initial departure from liquid saturation as the flow decompresses. The phase change rate limitations are due to both an absence of interfacial area and a lack of thermal driving potential. It is the initial nucleation process which generates the first interfacial area. This process takes place in the zone between the saturation line and the throat in the converging portion of the nozzle. Nucleation will occur generally at cavity defects on solid surfaces, these surfaces predominantly being wall area in small geometries having qualitatively large surface-to-volume ratio. As the geometry increases in size so that the surface-to-volume ratio increases, it is expected that bulk nucleation on imbedded impurities will become important. At this time, there is no definitive knowledge that the transition from wall-dominated to bulk-dominated nucleation will occur. In what follows, both processes are described, and later comparisons will show the effects of including the bulk nucleation process in geometries larger than those typical of bench-scale laboratory experiments.

Wall nucleation

The wall nucleation process is described in Shin & Jones (1993). The formation, growth and departure of a bubble from an active nucleation site are considered as a cyclical process consisting of two periods. During the bubble growth period the saturation temperature inside the bubble represents the boundary condition for a thermal wave to penetrate the wall.

During the waiting period after departure before the appearance of another nuclei at the site, superheated liquid contacts the wall resulting in a wall temperature between saturation and the

superheat temperature. This wall temperature then relaxes causing both the solid and liquid to become increasingly closer to the temperature represented by the liquid superheat. The next bubble is nucleated when the wall–liquid contact line temperature reaches the temperature corresponding to the saturation temperature inside a bubble of critical radius equal to the cavity size.

Critical size increases as the waiting period, t_w, decreases, corresponding to a lower contact-line wall superheat. If t_w vanishes, the maximum value of active cavity size, ($R_{c,max}$) is achieved due to the lack of time for the contact line to equilibrate towards the superheat temperature. This maximum value is independent of the flow conditions. This particular cavity size is a function only of the thermodynamic state of the particular fluid–solid system, and results in a minimum surface energy for the nuclei formed.

For the case where the dwell time, t_w, vanishes, the nucleation frequency at the cavity is also maximized. The departure size is, therefore, essential in determining the growth time, and hence the nucleation frequency. This departure size is determined from a balance of drag and surface tension forces. Analysis of the activation criterion and the departure size for the nuclei allowed nucleation frequencies to be obtained from the data. These were then correlated empirically with superheat as

$$f_{max} = 10^4 \Delta T_{sup}^3, \tag{37}$$

where f_{max} is the maximum nucleation frequency in hertz and $\Delta T_{sup} \equiv (T_L = T_V)$ is the liquid superheat in degrees Kelvin. This dimensional correlation provided the least scatter of any method examined and so was chosen over some, perhaps more desirable, dimensionless relationships.

The nucleation site density was then determined by assuming there is a maximum energy available for nucleation in the cylindrical disk of thickness $\delta = \frac{2}{3} R_c(\varrho_G/\varrho_L)$ having mass equal to that in the newly-formed vapor nucleus. Maximum nucleation site densities were thus determined for each data set and correlated empirically as

$$N_{ns}^* \equiv (2R_d)^2 N_{ns} = 10^{-7} R_c^{*-4} \quad \text{and so} \quad N_{ns} = 0.25 \times 10^{-7} \frac{R_d}{R_{cs}^4}, \tag{38}$$

where the superheat-based cavity size is given by

$$R_{cs} = \frac{2\sigma T_V}{\varrho_V \Delta i_{FG} (T_L - T_V)} \tag{39}$$

with σ the surface tension. The bubble departure radius was determined as

$$R_d^* \equiv \frac{R_d}{R_c} = \frac{0.818}{\sqrt{C_f}} \left(\frac{K^2}{We_{cL}}\right)^{5/14} \left(\frac{1}{Re_{cL}}\right)^{2/7}, \tag{40}$$

with We_{cL} and Re_{cL} the Weber and Reynolds numbers for a critical-sized bubble based on the liquid velocity. The dimensional form of this equation is

$$R_d = 0.58 K^{5/7} \left[\left(\frac{\sigma R_c}{\varrho_L}\right)^{1/2} \left(\frac{\mu}{\tau_w}\right)^{7/10} \left(\frac{1}{\nu}\right)^{3/10} \right]^{5/7}, \tag{41}$$

where the momentum diffusivity is ν and the wall shear was given by the Blasius relation

$$\tau_w = 0.079\, Re_D^{-0.25} \frac{\varrho_L w^2}{2}. \tag{42}$$

The coefficient K was used to consider the decrease in drag due to the nonsphericity of the departing nuclei but was taken as unity in all calculations. Equations [38]–[42] were combined to obtain

$$N_{ns} = 8.41 \times 10^{-9} \left[\left(\frac{T_V}{T_L - T_V}\right) \left(\frac{2\sigma}{\varrho_V \Delta i_{FG}}\right) \right]^{-23/7} \left[\left(\frac{\sigma}{\varrho_L}\right)^{1/2} \left(\frac{\mu_L}{\tau_0}\right)^{0.7} \left(\frac{\varrho_L}{\mu_L}\right)^{5/7} \right]^2. \tag{43}$$

Combination of the departure frequency per site with the site density yields the wall nucleation rate as

$$J_{wmax} = \frac{N_{ns} f_{max} \xi}{A}, \tag{44}$$

which in dimensionless terms becomes

$$J^*_{\text{wmax}} \equiv \frac{J_{\text{wmax}} R^4}{w_L} = 1.296 \times 10^2 \left(\frac{\varrho_V}{\varrho_L}\right)^2 H^*(z) \frac{\varrho_L c_{pL} \Delta T^2_{\text{sup,t}} R^3_N}{\sigma T_{\text{sat}} L^2_N} \text{Re}_D^{3/4}. \quad [45]$$

Due to the specific shape of a linear nozzle, the geometric function $H^*(z)$ becomes

$$H^*(z) = \frac{z}{R_N}\left[1 - 2.75\left(\frac{\Delta R}{R_N}\right)\left(\frac{z}{L_N}\right)\right]. \quad [46]$$

It should be noted that experiments in small geometries having diameters of the order of 10^{-2} m were used to develop the equations for the wall nucleation rate identified above. Under these conditions, experiments have shown that wall nucleation dominates. Wall nucleation was assumed to occur in the region between the saturation line and the location of maximum superheat—the transition from a converging to diverging or straight nozzle section. After this point, bulk flashing is assumed to occur and the wall assumed to be at saturation, precluding nucleation.

Bulk heterogeneous nucleation

A model for heterogeneous nucleation in the bulk fluid was developed by Soplenkov & Blinkov (1983). The assumption was that the liquid always carried suspended particles whose size distribution is $n(\delta)$. At nucleation sites, only supercritical particles $\delta > \delta^*$ can be active, where δ^* is the diameter of the critical spherical vapor nucleus and depends on the physical properties of the liquid and degree of metastability. Thus, the total number of nucleation sites where evaporation and bubble formation can occur is

$$N_B(\text{Gi}) = \int_\infty^{\delta^*} n(\delta)\, d\delta, \quad [47]$$

where Gi is the Gibbs number (Skripov 1982). An empirical correlation for $N_B = N_B(\text{Gi})$ was obtained using experimental data on the blowdown of initially subcooled water through short tubes $4 \leqslant L/D \leqslant 10$, $L \leqslant 0.3$ m, with sharp entrances where $\text{Gi} \geqslant 1500$. The result was

$$\log(N_B) = 12.5 - 0.15 \log(\text{Gi}). \quad [48]$$

The nucleation source term for the numerical model is thus obtained as

$$J_B = \frac{dN_B}{dt} = \frac{N_B(\text{Gi}) w}{\Delta z}, \quad [49]$$

where Δz is the mesh spacing. The overall concept of bulk nucleation is that the process is "sudden," having a characteristic time $\Delta\tau = \Delta x/w$. Thus, the source term is taken to be zero everywhere except for that mesh cell corresponding to the transition from a converging to diverging (or straight) geometry, consistent with maximum superheat at this location. Bulk nucleation thus vanishes everywhere except for the throat cell, and in this cell is additive to the continuous wall nucleation determined from the model of Shin & Jones (1993).

Numerical Methods

For solving the equations given by [1]–[5], a semi-implicit method (EPRI 1983) is used having the Courant stability criterion

$$\Delta t \leqslant \frac{\Delta z}{w_{\max}}, \quad [50]$$

which significantly increases the allowable time step compared with explicit methods and makes use of the microcomputer feasible. The channel is divided into a number of cells with uniform spatial mesh spacing, Δx. All thermodynamic variables are cell-centered, whereas velocities are computed at cell faces.

As an illustration, the finite-difference form developed for the vapor mass conservation equation is

$$(\epsilon^{n+1}\varrho_V^{n+1} - \epsilon^n \varrho_V^n)_i + \frac{1}{A_i}\frac{\Delta t}{\Delta x}\left[(\epsilon^n \varrho_V^n w^{n+1} A)_{i+1/2} - (\epsilon^n \varrho_V^n w^{n+1} A)_{i-1/2}\right] = \Gamma_V^{n+1} \Delta t. \quad [51]$$

Relationships between the cell-edge and cell-center variables used are based on full donor cell differencing, which is known to be extremely stable, resulting in

$$\psi_{i+1/2} = \begin{cases} \psi_i & \text{if } w_{i+1/2} \geqslant 0 \\ \psi_{i+1} & \text{if } w_{i+1/2} < 0, \end{cases} \tag{52}$$

where $[\psi]^T \equiv [\varrho_V, \varrho_L, u_L, \epsilon, N_B]$. Other equations are treated identically.

The equation of motion has the form

$$w_{i+1/2}^{n+1} = -\beta_{i+1/2}^n (p_{i+1}^{n+1} - p_i^{n+1}) + j_{i+1/2}^n, \tag{53}$$

where $\beta_{i+1/2}^n$ and $j_{i+1/2}^n$ are calculated at the old time step and have the form

$$\beta_{i+1/2} = \frac{\Delta t}{\Delta x} \left[\frac{1}{\varrho_M^n + K^n \Delta t |w^n|} \right]_{i+1/2} \tag{54}$$

and

$$j_{i+1/2} = \varrho_M^n w_{i+1/2}^n \left[1 - \frac{\Delta t}{\Delta x} (w_{i+3/2}^n - w_{i-1/2}^n) \right] \left[\frac{1}{\varrho_M^n + K^n \Delta t |w^n|} \right]_{i+1/2}, \tag{55}$$

and where

$$K^n = f_f(w^n |w^n|). \tag{56}$$

Using [53] the number of variables is reduced by one where equations with the velocity $w_{i+1/2}^{n+1}$ appear.

The overall system of equations [1] written in a partially implicit form represents a nonlinear algebraic equation set for all unknown variables at the new time step. The system is solved using the Newton iteration shown in the following equation. The v-superscript indicates successive iterative approximations to variables at the new time step with superscript $n+1$. All equations are linearized by Taylor's expansion about the latest iteration values of the unknowns. The linearized form of [51] is

$$\begin{aligned} \Delta p_i^v \Bigg\{ \left(\epsilon \frac{d\varrho_V}{dp} \right)_i^v + \frac{1}{A} \frac{\Delta t}{\Delta x} (\epsilon_{i+1/2}^n \varrho_{V_{i+1/2}}^n A_{i+1/2} \beta_{i+1/2}^n + \epsilon_{i-1/2}^n \varrho_{V_{i-1/2}}^n A_{i-1/2} \beta_{i-1/2}^n) \\ - \left(\frac{\partial \Gamma_V}{\partial p} \right)_i^v \Delta t \Bigg\} + \Delta \epsilon_i^v \left[\varrho_{V_i}^v - \left(\frac{\partial \Gamma_V}{\partial \epsilon} \right)_i^v \Delta t \right] - [(1-\epsilon)_i^v \Delta T_{L_i}^v] \left(\frac{\partial \Gamma_V}{\partial T_L} \right)_i^v \frac{\Delta t}{(1-\epsilon)_i^v} \\ - \left(\Delta p_{i+1}^v \frac{1}{A_i} \frac{\Delta t}{\Delta x} \epsilon_{i+1/2}^n \varrho_{V_{i+1/2}}^n A_{i+1/2} \beta_{i+1/2}^n \right) \left(\Delta p_{i-1}^v \frac{1}{A_i} \frac{\Delta t}{\Delta x} \epsilon_{i-1/2}^n \varrho_{V_{i-1/2}}^n A_{i-1/2} \beta_{i-1/2}^n \right) \\ = \left\{ (\epsilon^v \varrho_V^v - \epsilon^n \varrho_V^n) + \frac{1}{A} \frac{\Delta t}{\Delta x} [(\epsilon^n \varrho_V^n w^v A)_{i+1/2} - (\epsilon^n \varrho_V^n w^v A)_{i-1/2}] - \Gamma_{V,i}^v \Delta t \right\}. \end{aligned} \tag{57}$$

In matrix form, the equation set may be written as

$$- \begin{bmatrix} B_1 \\ B_2 \\ B_3 \\ B_4 \end{bmatrix} \Delta p_{i-1}^v + \mathbf{H}_{4\times 4} \begin{bmatrix} \Delta p_i^v \\ (1-\epsilon)_i^v \Delta T_{L_i}^v \\ \Delta \epsilon_i^v \\ \Delta N_i^v \end{bmatrix} - \begin{bmatrix} C_1 \\ C_2 \\ C_3 \\ C_4 \end{bmatrix} \Delta p_{i+1}^v = \begin{bmatrix} D_1 \\ D_2 \\ D_3 \\ D_4 \end{bmatrix}; \tag{58}$$

$\mathbf{H}_{4\times 4}$ is a 4×4 matrix. If [58] is multiplied by the inverse of $\mathbf{H}$ the result is

$$\mathbf{H}^{-1} \begin{bmatrix} B_1 \\ B_2 \\ B_3 \\ B_4 \end{bmatrix} \Delta p_{i-1}^v + \begin{bmatrix} \Delta p_i^v \\ (1-\epsilon)_i^v \Delta T_{L_i}^v \\ \Delta \epsilon_i^v \\ N_i^v \end{bmatrix} - \mathbf{H}^{-1} \begin{bmatrix} C_1 \\ C_2 \\ C_3 \\ C_4 \end{bmatrix} \Delta p_{i+1}^v = \mathbf{H}^{-1} \begin{bmatrix} D_1 \\ D_2 \\ D_3 \\ D_4 \end{bmatrix}. \tag{59}$$

The first of the four equations involves the corrections Δp^{ν}_{i-1}, Δp^{ν}_{i} and Δp^{ν}_{i+1}, only where

$$K_i \Delta p^{\nu}_{i-1} + \Delta p^{\nu}_{i} + L_i \Delta p^{\nu}_{i+1} = M_i. \qquad [60]$$

The system of equations in [60] written in each mesh cell from 1 to N is tridiagonal:

$$\begin{bmatrix} 1 & L_1 & & & & & & & \\ K_2 & 1 & L_2 & & & & & & \\ & K_3 & 1 & L_3 & & & & & \\ & & & \cdots & & & & & \\ & & & & \cdots & & & & \\ & & & K_{N-2} & 1 & L_{N-2} & & & \\ & & & & K_{N-1} & 1 & L_{N-1} & & \\ & & & & & K_N & & (1+L_N) & \end{bmatrix} \cdot \begin{bmatrix} \Delta p^{\nu}_1 \\ \Delta p^{\nu}_2 \\ \Delta p^{\nu}_3 \\ \vdots \\ \vdots \\ \Delta p^{\nu}_{N-2} \\ \Delta p_{N-1} \\ \Delta p^{\nu}_N \end{bmatrix} = \begin{bmatrix} M_1 \\ M_2 \\ M_3 \\ \vdots \\ \vdots \\ M_{N-2} \\ M_{N-1} \\ M_N \end{bmatrix} . \qquad [61]$$

The solution of [34] gives the corrections Δp^{ν}_i. Knowing these corrections, we get $\Delta \epsilon^{\nu}_i$, $\Delta T^{\nu}_{L_i}$ and ΔN^{ν}_i from [59]. These corrections will then be added to p^{ν}_i, ϵ^{ν}_i, $T^{\nu}_{L_i}$ and N^{ν}_i, and the iterative process repeated until the condition $\max(\Delta p^{\nu}_i / p_i) < \alpha$ is satisfied, where α is a sufficiently small number. The present case used $\alpha = 10^{-3}$, which resulted in converged results (smaller values of α producing negligible change) requiring 3–4 iterations per time step.

Boundary Conditions

In general, we can say that the numerical solution to the problem was pressure-forced. That is, the inlet pressure boundary condition is given along with the stagnation inlet state of the fluid and an assumption of vanishing void fraction and bubble number density at the throat and an assumption that the flow was choked (i.e. exit downstream pressure sufficiently low). The balance of the results are computed as described. Boundary conditions were achieved by adding additional cells with the subscripts 0 and $N+1$. For subsonic flow through the inlet boundary the relations $K_1 \Delta p^{\nu}_0 + \Delta p^{\nu}_1 + L_1 \Delta p^{\nu}_2 = M_1$ with $p_0 = \text{const}$ and $\Delta p^{\nu}_0 = 0$ were utilized. In addition to the condition on p_0, we impose initial liquid temperature T_{L0} equal to the inlet value, and an inlet void fraction and bubble number density equal to zero. The inlet velocity w_0 was determined by linear extrapolation upstream based on computed results.

For subsonic flow through the outlet boundary,

$$\left.\begin{aligned} K_N \Delta p^{\nu}_{N-1} + \Delta p^{\nu}_N + L_N \Delta p^{\nu}_{N+1} &= M_N \\ p_{n+1} = p_\infty = \text{const} \quad \text{and} \quad \Delta p^{\nu}_{N+1} &= 0. \end{aligned}\right\} \qquad [62]$$

The values of ϵ^{ν}_{N+1}, $T^{\nu}_{L_{N+1}}$ and N^{ν}_{N+1} were determined by linear extrapolation downstream based on computed results. If the flow through the outlet boundary was supersonic, it was assumed that $\Delta p^{\nu}_{N+1} = \Delta p_N$, and then all variables in the $N+1$ cell were linearly extrapolated downstream.

3. RESULTS AND DISCUSSION

Numerical Results

The experience with the computations was reasonably good from the viewpoint of using a microcomputer for the calculations. The entire program required approximately 80 kB of main memory on the HP-9816S. Cell lengths required for stable, converged results in typical calculations were 5 mm for the BNL geometry (Abuaf *et al.* 1981), representing 110 cells, and ~2.5 mm for the Marviken geometry (EPRI 1982) (40–70 cells) and for the geometry of Sozzi & Sutherland (1975) (64 cells, results not shown).

The computational times required to reach a steady-state solution usually took 200–300 time steps with each time step requiring ~4 internal iterations in the early stages of solution and 1–2 iterations near steady state. A single iteration required approx. 40 s so that calculation times were 8–10 h. A typical case was set up during the day and run overnight with the results ready the next morning. Since the computer was completely dedicated to the problem, there was no difficulty in

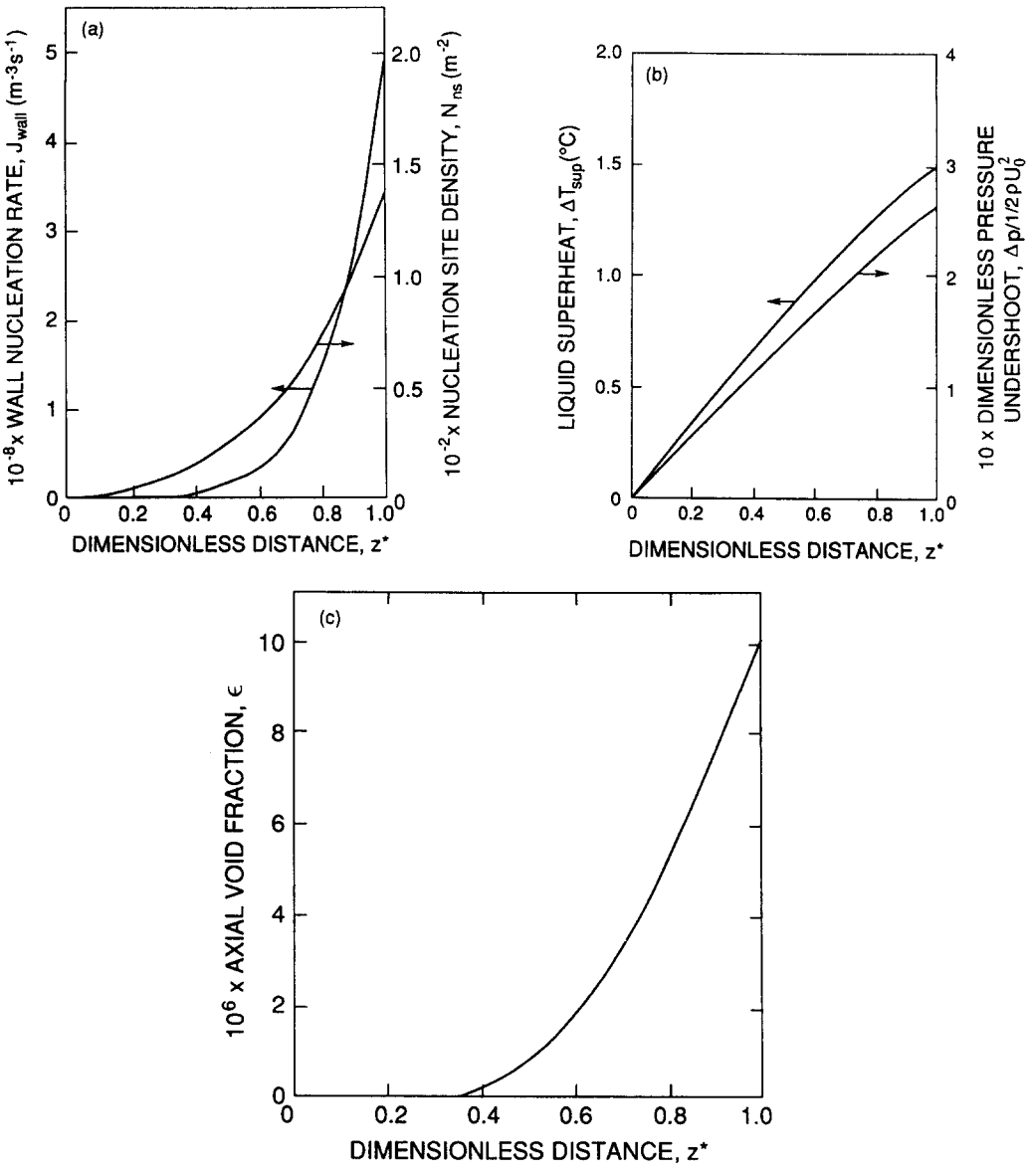

Figure 2(a–c). Calculations for the nucleation zone for the conditions of Ardron & Ackerman (1978), Run C35 (T_{in} = 111.5°C, p_{in} = 1.59 bar, G = 7740 kg/s-m^2, ΔT_{sup} = 1.66 K).

undertaking computations in this manner. Moreover, it would be expected that newer and faster microcomputers would require significantly less time for the same calculations.

Comparison with the Experimental Results

Void development at the throat

In virtually all previous flashing models, the nucleation zone is treated as a single point of flashing inception. This has been justified since the zone of supersaturation in many cases is quite narrow. However, in this zone, the voids which develop from the nuclei form the basis for interfacial mass transfer and subsequent growth downstream. It is, therefore, important that both the size and number be determined so that accurate calculations of void development may be undertaken.

Calculations were made for all runs reported by Bailey (1951), Brown (1961), Sozzi & Sutherland (1975), Ardron & Ackerman (1978), Abuaf *et al.* (1981) and Celata *et al.* (1982). The two cases with the smallest and largest calculated throat void fractions are shown in figures 2 and 3. The smallest void fraction was computed for the Ardron & Ackerman (1978) run C25 having a superheat at the throat of 1.66 K with 1.6 bar inlet pressure. As seen in figure 2(a), while the

nucleation site density increased to approx. 140 m^{-2} with overall bulk-equivalent wall nucleation rates to about $5 \times 10^8\ m^{-3}\ s^{-1}$, the void fraction increased only to $\sim 10^{-5}$ [figure 2(c)].

The case with the largest computed throat void fraction was Run 39 from the data of Brown (1961) (figure 3), having a throat superheat of 81.6 K, an inlet pressure of 68.4 bar and a computer bulk-equivalent wall nucleation rate at the throat of slightly less than $5 \times 10^{22}\ m^{-3}\ s^{-1}$, 14 orders of magnitude larger than that of Ardron & Ackerman (1978). In this case, the throat void fraction increased to 0.009. This value is also negligibly small and provides confirmation of the original hypothesis of Abuaf *et al.* (1980, 1983). This further explains why the critical flow rates of all these runs can be accurately confirmed (within ~3%) by correctly predicting the throat pressure through the superheat and then assuming single-phase flow.

Void development downstream—small nozzles

Calculations for the long, vertical nozzle in the experiments of Abuaf *et al.* (1981) taken at Brookhaven National Laboratory (BNL) are shown in figure 4. In figure 4(a) comparisons are shown between calculated void fraction and pressure profiles and those measured in the experiment.

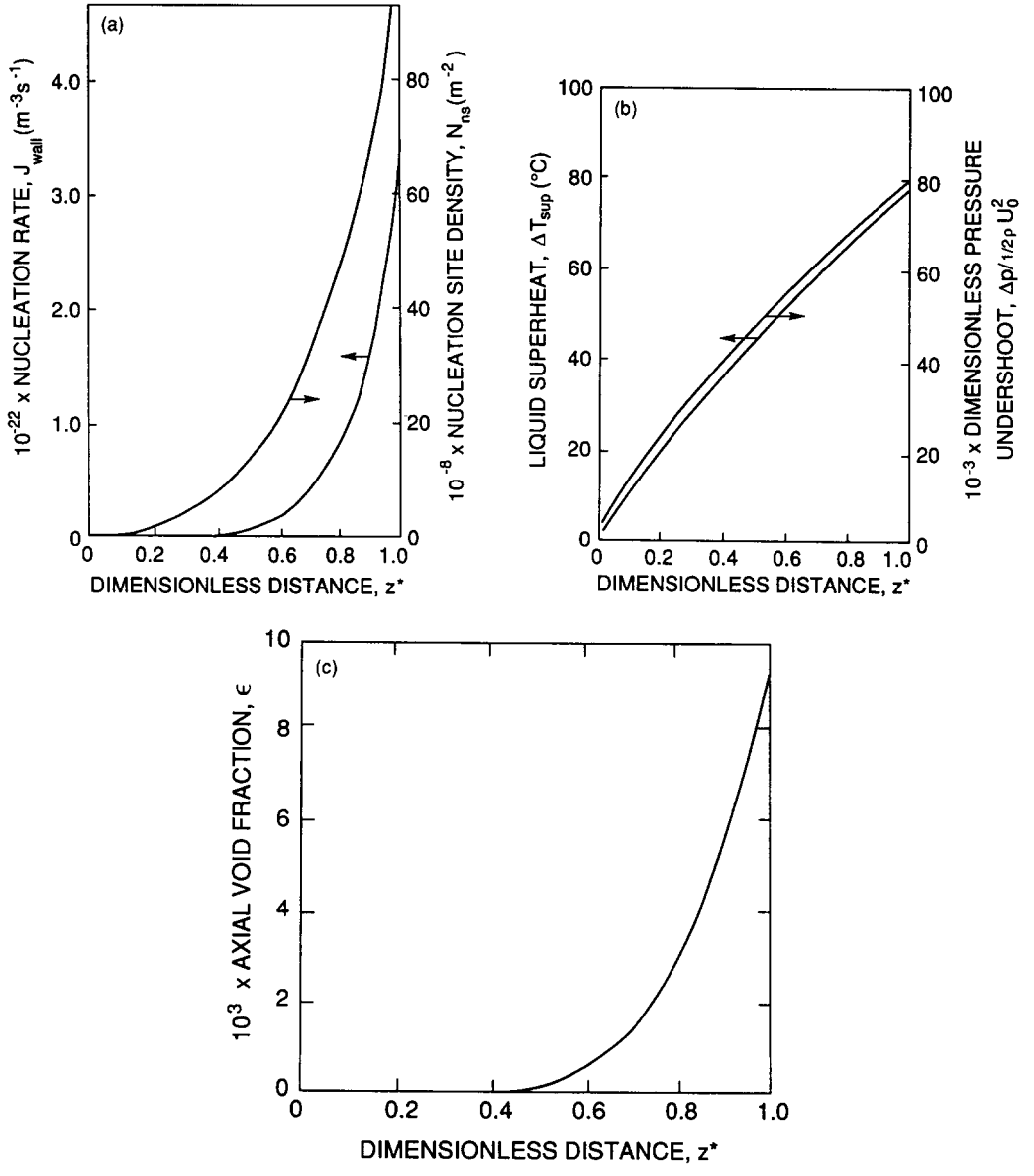

Figure 3(a–c). Calculations for the nucleation zone for the conditions of Brown (1961), Run 39 ($T_{in} = 280°C$, $p_{in} = 1.59$ bar, $G = 303$ kg/s-m^2, $\Delta T_{sup} = 81.6$ K).

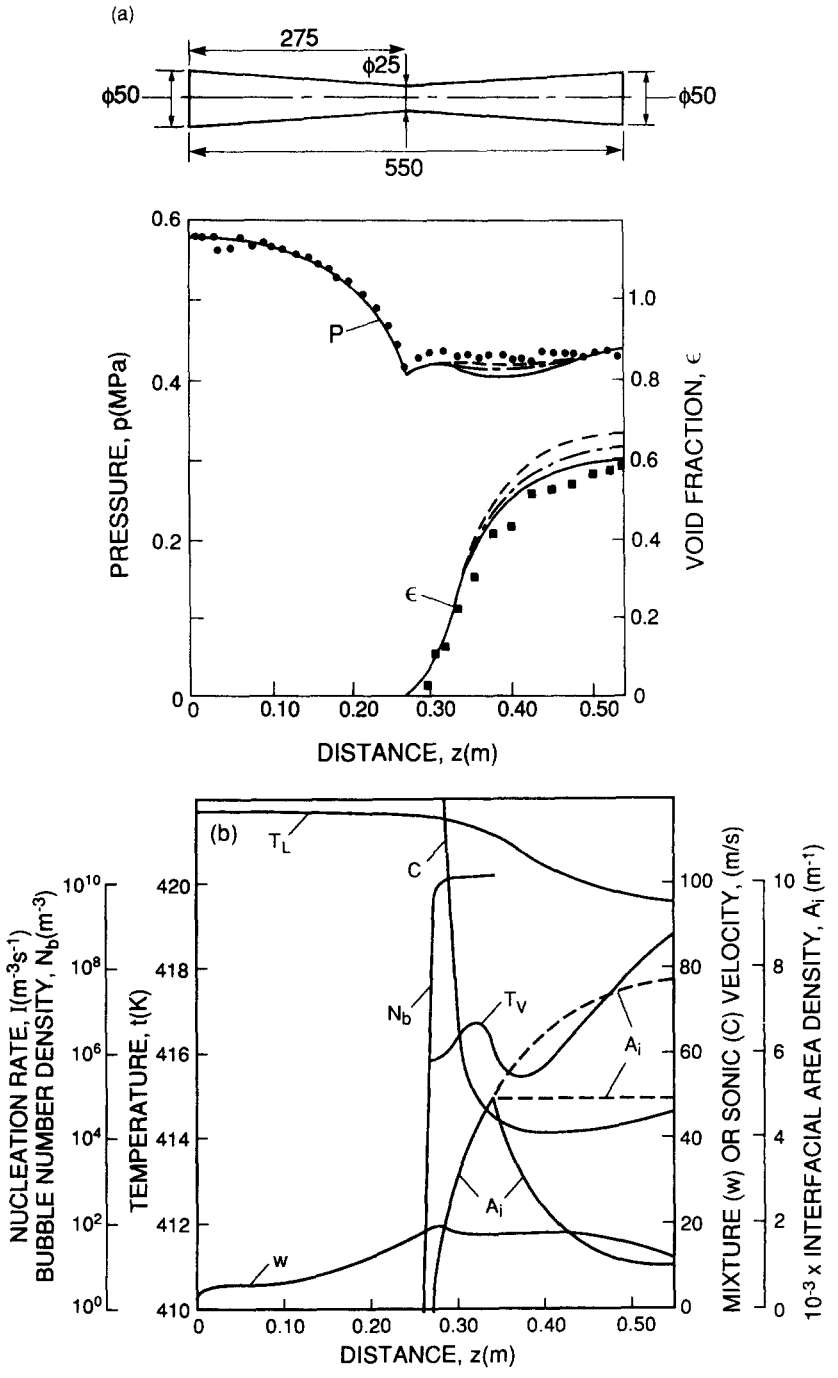

Figure 4. Comparison between experimental and calculated distributions of pressure and void fraction and other void development parameters for the BNL nozzle Run 273 (Abuaf *et al.* 1981) ($p_0 = 0.573$ MPa, $T_0 = 421.85$ K, $\Delta T_0 = 8.4$ K, $\dot{m}_{exp} = 8.71$ kg/s, $\dot{m}_{calc} = 8.8$ kg/s, $p_\infty = 0.442$ MPa): ——, flow regime map 1; —·—, flow regime map 2; – – –, bubbly model exclusively. (a) Pressure and void distributions; (b) void development parameters.

In figure 4(b) curves are included showing the liquid temperature, T_L, vapor temperature, T_V, interfacial area density, A_i, mixture velocity, w, bubble number density in the region up to 30% voids, log(N), and local frozen sonic velocity, c.

In all these calculations, it was confirmed that the calculated effect of bulk nucleation based on [48] was negligible. This lends additional support to the experimental evidence that for nozzles of

this small diameter wall nucleation predominates. Note also that the correlations which are used to calculate the wall nucleation rate were based on this assumption.

Three methods of calculation were used to make these calculations shown in figure 4:

1. Flow regime 1 consisting of bubbly, bubbly–slug, transitional and dispersed flows (— · —).
2. Flow regime 2 consisting of bubbly, transitional churn turbulent and dispersed flows.
3. Bubbly flow for any void fraction (– – –).

One can see that the three calculated values of void fraction in figure 4(a) differ slightly due to the differing interfacial area density for phase change. Bubbly flow gives the highest void calculated, since the interfacial area density is the largest. Model flow regime 1 gives a smaller void fraction since the area density is lower and decreases after $\epsilon = 0.3$ [figure 4(b)]. For the third model, flow regime 2, the interfacial area density is constant after $\epsilon = 0.3$, but the void fraction is still lower. This is because as seen in the pressure profiles, this third model results in increased superheat offsetting the effect of reduced interfacial area density.

While the void fraction in the latter case is closer to the data, the pressure profiles are further away. The reasons for these results are unknown but show both the need for careful modeling of the surface area density and for more definitive experiments to delineate the type of behavior to be expected.

Figures 5–7 show similar results for different BNL runs having the conditions summarized in table 1 (the conditions for Run 273 are summarized in the caption to figure 4). In these cases, only the bubbly flow regime results are shown. Table 2 compares the exit void fraction for the bubbly flow calculation compared with that for the flow regime 1 results in comparison with the data. It is seen that in all cases, the inclusion of a more realistic flow regime calculation, which considers the reduction in interfacial area density due to agglomeration, produces results closer to the data.

Critical flow of saturated water through a Laval nozzle having a throat diameter of 3.84 mm is shown in figure 8 for the data of Karasev *et al.* (1977). In this case, wall nucleation dominates bulk nucleation by 2 orders of magnitude, again affirming that this is the predominant mode of void formation in the nucleation zone in small geometries. It is seen that the flow becomes overexpanded and goes supersonic downstream of the throat. Substantial expansive cooling of both liquid and vapor are seen. Similar results are obtained for all the subcooled inlet runs of Sozzi & Sutherland (1975).

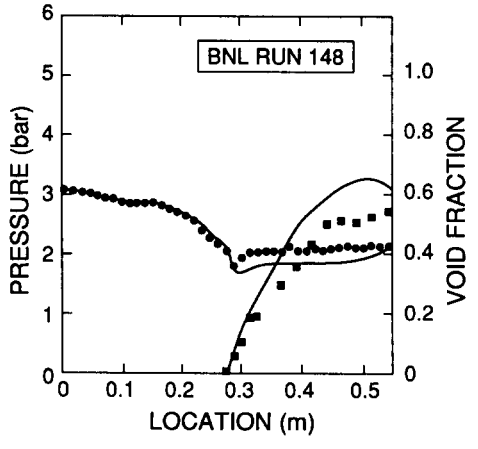

Figure 5. Comparison between experimental and calculated distributions of pressure and void fraction and other void development parameters for the BNL nozzle Run 148 (Abuaf *et al.* 1981) ($p_0 = 3.05$ bar, $T_0 = 384.35$ K, $\Delta T_0 = 12.80$ K, $\dot{m}_{exp} = 7.50$ kg/s, $\dot{m}_{calc} = 7.8$ kg/s, $p_\infty = 2.06$ bar).

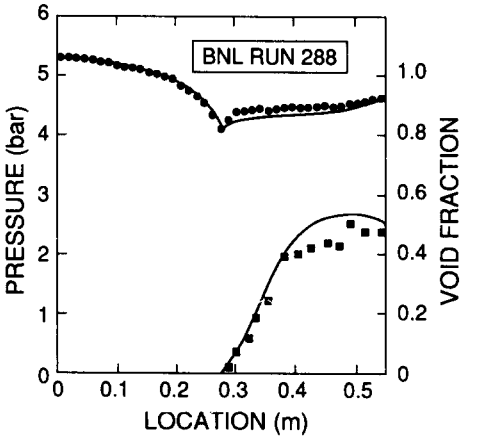

Figure 6. Comparison between experimental and calculated distributions of pressure and void fraction and other void development parameters for the BNL nozzle Run 288 (Abuaf *et al.* 1981) ($p_0 = 5.3$ bar, $T_0 = 422.35$ K, $\Delta T_0 = 4.8$ K, $\dot{m}_{exp} = 7.25$ kg/s, $\dot{m}_{calc} = 7.27$ kg/s, $p_\infty = 4.591$ bar).

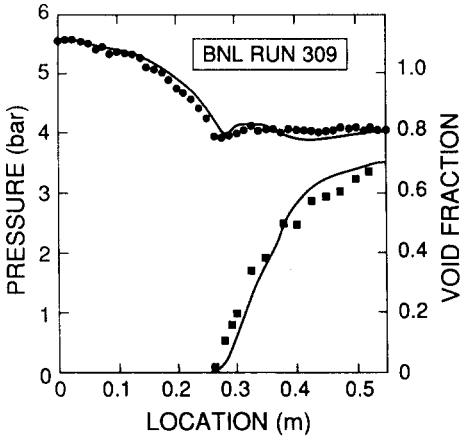

Figure 7. Comparison between experimental and calculated distributions of pressure and void fraction and other void development parameters for the BNL nozzle Run 309 (Abuaf *et al.* 1981) ($p_0 = 5.559$ bar, $T_0 = 422.25$ K, $\Delta T_0 = 6.75$ K, $\dot{m}_{exp} = 8.80$ kg/s, $\dot{m}_{calc} = 8.23$ kg/s, $p_\infty = 4.05$ bar).

Void development downstream—large nozzles

Figure 9 shows calculations for a round-entrance, large-diameter ($D = 0.51$ m) pipe used in Marviken experiments (EPRI 1982). The single point at the inlet represents the measured inlet pressure used to drive the flow calculations. In figure 9(a) results are shown with $J_B = 0$, no bulk nucleation. Figure 9(b) shows calculations where the bulk nucleation model is included. The number density is substantially larger in the early stages of decompression near the inlet when bulk nucleation is included and the voids begin to grow earlier in the nozzle but little effect on the temperatures or pressures is seen. However, near the exit where void development becomes significant, the number densities approach each other and void growth becomes similar. This shows that in the larger geometries, as the volume-to-surface ratio increases, the role of bulk nucleation can be expected to become increasingly important.

Figure 10 shows the effects of bulk nucleation in a comparison between calculated and experimental critical mass flow rates of the Marviken experiments having the same diameter as that of figure 9 (stagnation temperature, $T_0 = \text{const}$). It is obvious from this case that the inclusion of bulk nucleation for this larger geometry substantially improves the prediction of the critical flows, due mainly to improved computation of void development. In this case, accurate calculation is crucial since the flow rate is void dominated.

For the case of transient flow calculations in large nozzles, the computed results for Marviken agree well with the experimental values (figures 11 and 12) up to about 30 ms, after which the liquid temperature begins to become affected by the nonuniformity in the vessel temperature. Again this indicates the effect of the inclusion of bulk nucleation in the overall process of the initial generation of bubble nuclei.

It has long been common wisdom that nonequilibrium becomes increasingly important as the length of nozzles becomes shorter and shorter with respect to the diameter. The converse is also considered true. These concepts are confirmed in figure 13, which shows that as the L/D ratio of the nozzle increases, the flow and the model approach that calculated by homogeneous equilibrium, giving a further indication of the lack of importance of mechanical nonequilibrium under these circumstances.

Table 1. Summary of conditions for the BNL experiments (Abuaf *et al.* 1981)

BNL Run	p_0 (bar)	T_0 (K)	ΔT_0 (K)	p_∞ (bar)	$\dot{m}_{meas}$ (kg/s)	$\dot{m}_{calc}$ (kg/s)
148	3.05	394.35	12.80	2.06	7.50	7.80
288	5.30	422.35	4.80	4.591	7.25	7.27
309	5.559	422.25	6.75	4.05	8.80	8.23

Table 2. Comparison of calculated and experimental values of exit void fraction for the BNL data

BNL Run	Bubbly flow only	Flow regime map 1	Measured void data
148	0.66	0.59	0.55
273	0.69	0.61	0.57
288	0.52	0.49	0.49
309	—	0.71	0.70

Model 1 is bubbly flow only; model 2 is for flow regime map 1.

4. CONCLUSIONS

A computational framework for calculating the behavior of flowing, initially subcooled liquids in pipes and nozzles has been described for use on a microcomputer. The model uses the new distributed nucleation model of Shin & Jones (1993) coupled with a previous model for bulk nucleation developed by Soplenkov & Blinkov (1983) to determine appropriate initial conditions for flashing and void development downstream of the throat. The model, a five-equation, mechanical equilibrium (no slip), thermal nonequilibrium model incorporates recent advances in the theory of distributed wall nucleation in small ducts, as well as a previously developed model for bulk nucleation on suspended particles in larger geometries.

The model consisted of mixture and vapor mass conservation equations, a mixture momentum equation, the liquid energy equation and a bubble transport equation. Spherical bubble growth was calculated by traditional thermally-limited growth methods using local superheat. For closure, a relatively simple two-phase wall friction model was utilized, represented by a friction multiplier having different formulations in four different regions of void fraction.

Semi-implicit methods were used for differencing with all properties computed at the cell centers, and a donor cell method was used to calculate convective flux effects with velocities computed at cell boundaries. The system was solved by Newton iteration. Typical computational times on a Hewlett-Packard 9816 microcomputer based on the MC-68000 processor chip at 8 MHz were

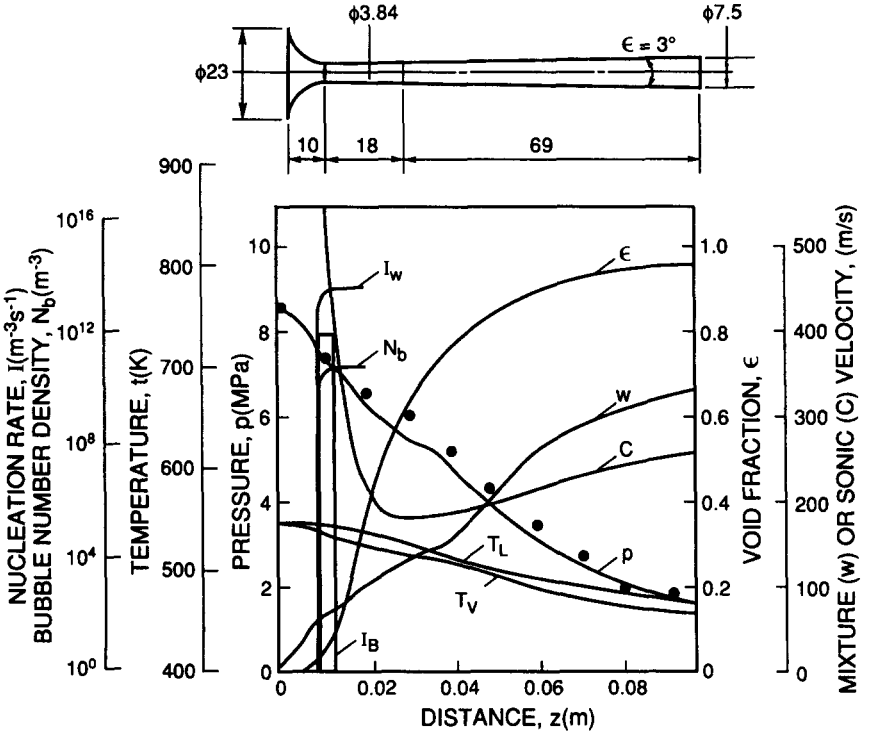

Figure 8. Calculated distributions of pressure and void fraction and other void development parameters for the small-scale Laval nozzle of Karasev *et al.* (1977) ($p_0 = 8.5$ MPa, $T_0 = 572$ K, $\Delta T_0 = 0$ K, $\dot{m}_{exp} = 0.535$ kg/s, $\dot{m}_{calc} = 0.575$ kg/s), ●, experimental pressure data.

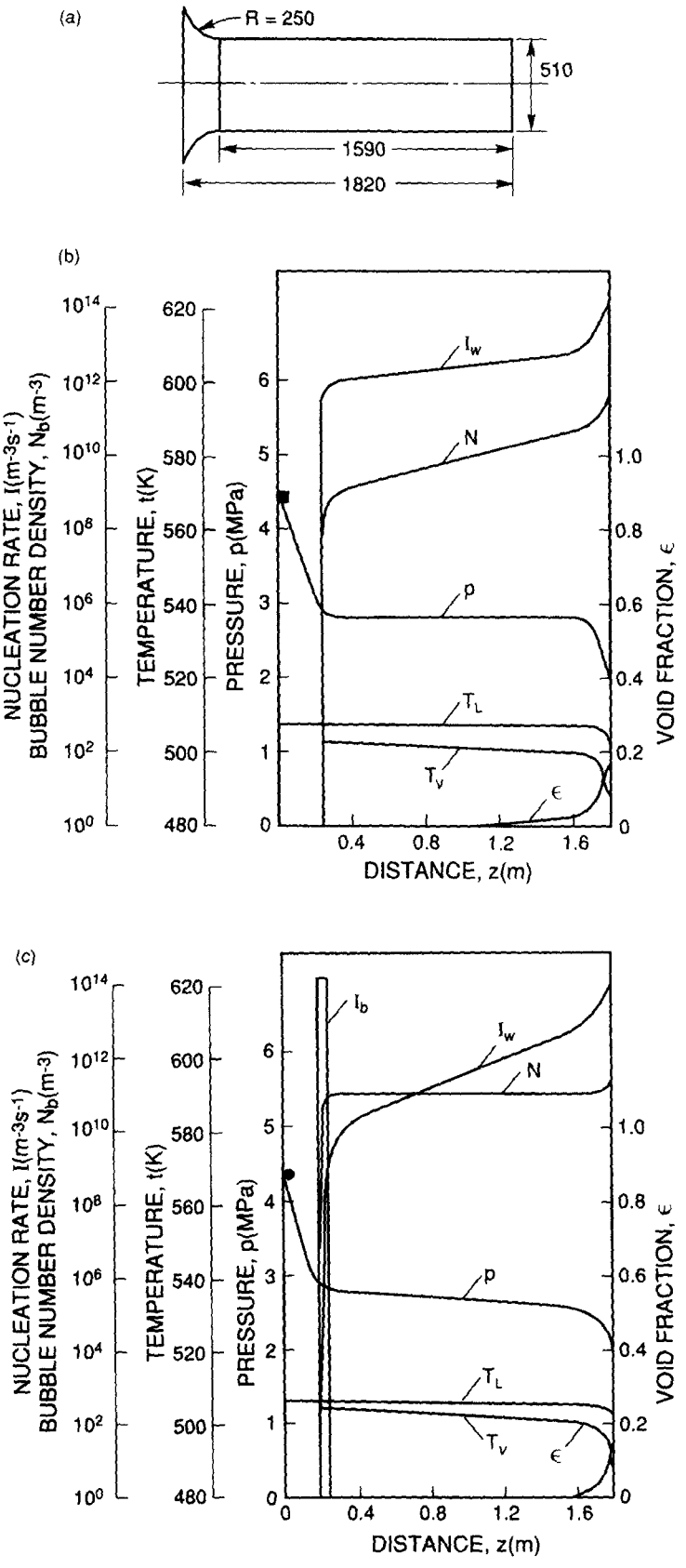

Figure 9(a–c). Calculated distributions of pressure and void fraction and other void development parameters for a Marviken nozzle with $L = 1.59$ m, $D = 0.51$ m and $L/D = 3.1$ (EPRI 1982) ($p_0 = 4.52$ MPa, $T_0 = 507.15$ K, $\Delta T_0 = 23.85$ K, $G_{exp} = 51{,}000$ kg/s-m^2, $G_{calc} = 55{,}280$ kg/s-m^2).

40–45 s/time step and a total of 8–10 h for a converged solution with all variables within 1 part in 10^3. In general, both qualitative and quantitative agreement was found between the data and computations. For small geometry, bulk nucleation has negligible effect all data examined. For large geometry, bulk nucleation adds an important component necessary for accurate determination of the interfacial area density (necessary for phase change and resultant void development).

While pressure profiles were best predicted by bubbly flow methods for all void fractions, the void profile were best predicted using a bubbly–churn–dispersed model which is felt to calculate the interfacial area density more appropriately. Some work obviously still needs to be accomplished in this area to bring the calculations into alignment with the magnitude and trends for all variables. The deficiency is thought to be in the computation of the interfacial area density.

Void fractions at the throat in nozzles were found to be negligible in all cases examined, which includes most experiments of subcooled inlet critical flashing flows described in the literature. This confirms previous hypotheses of Abuaf *et al.* (1980, 1983) and provides a powerful means of obtaining confirmatory computations of critical flow rates in such situations by computing equivalent single-phase flows based on the computed bulk superheat at the throat.

It was shown that careful attention must be paid to the modeling of the interfacial area density. For two-phase flows of initially subcooled liquids, the generation of interfacial area required for phase change begins as a nucleation process. Both wall and bulk nucleation processes are important, the former predominating the "small" geometries, the latter in "larger" geometries. An

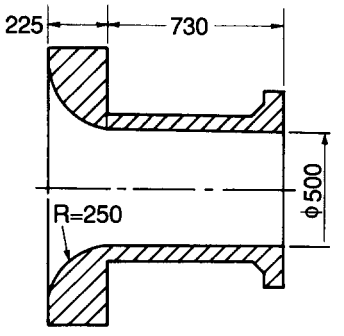

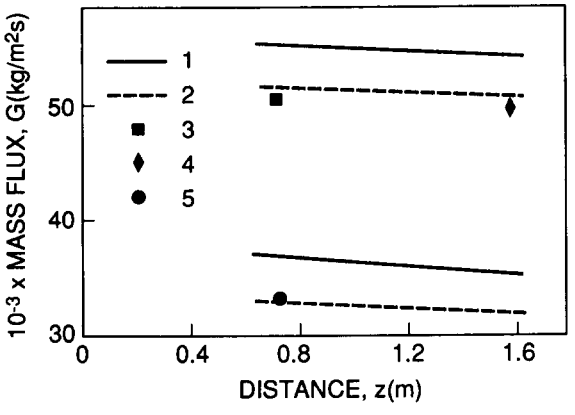

Figure 10. Comparison between calculated and experimental critical mass fluxes for large-diameter ($D = 0.51$ m), rounded-entrance Marviken nozzles (EPRI 1982): (1) calculation with wall nucleation only; (2) calculation with both wall and bulk nucleation; (3) $p_0 = 4.52$ MPa, $T_0 = 507$ K; (4) $p_0 = 4.52$ MPa, $T_0 = 507$ K; (5) $p_0 = 3.56$ MPa, $T_0 = 507$ K.

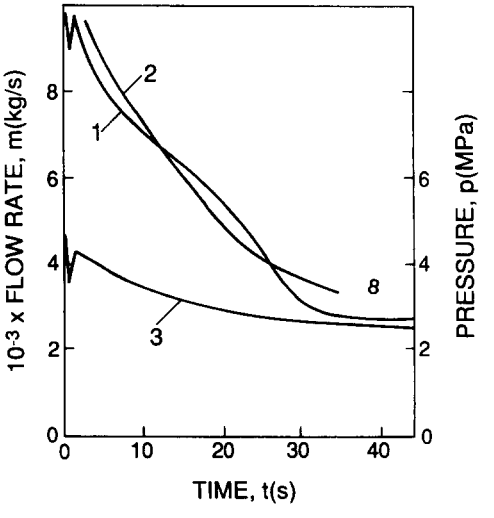

Figure 11. Blowdown in the Marviken nozzle experiment (EPRI 1982), $L = 0.955$ m, $D = 0.5$ m: (1) experimental flow rate; (2) flow rate calculation; (3) experimental pressure history.

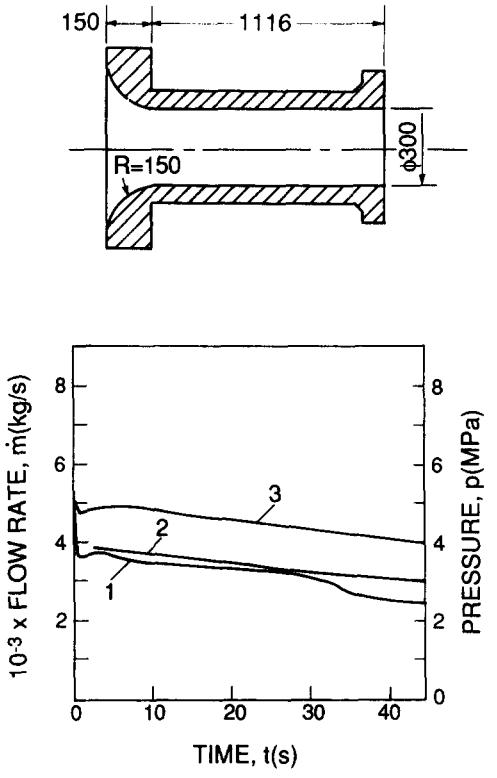

Figure 12. Blowdown of the Marviken nozzle experiment (EPRI 1982), $L = 1.226$ m, $D = 0.3$ m: (1) flow rate from experiment; (2) flow rate from calculation; (3) experimental pressure history.

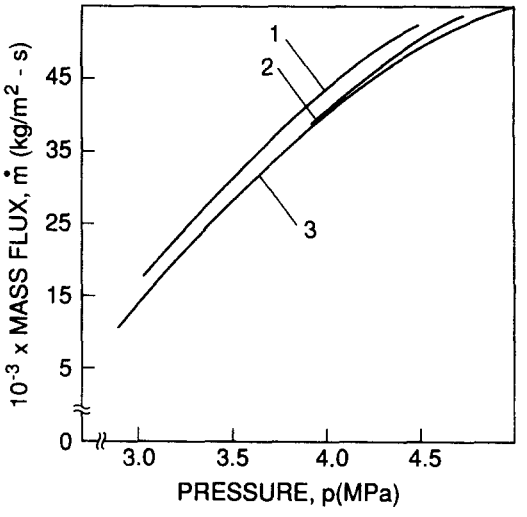

Figure 13. Critical flow for different size Marviken nozzles (EPRI 1982): (1) model presented, $D = 0.5$ m, $L = 0.955$ m and $L/D = 1.91$; (2) model presented, $D = 0.3$ m, $L = 1.266$ m and $L/D = 4.22$; (3) homogeneous equilibrium.

accurate balance of the two is necessary to obtain proper starting conditions for downstream void development, these conditions requiring both the number and sizes of nucleated bubbles. At this point, it is not known exactly what is meant by the two words "small" and "large" except as they relate to the surface-to-volume ratio of the geometry in question. For the computations described herein, both qualitative and quantitative agreement was found for downstream void development in comparison with the existing data, indicating that the nucleation models utilized appear adequate.

The nonequilibrium model upon which these calculations and comparisons were based did not utilize any assumption regarding thermal nonequilibrium. Rather, the degree of thermal nonequilibrium obtained in each situation was the result of the nucleation and bubble growth models combined with appropriate conservation laws for mass and energy. Furthermore, the calculations herein utilized a no-slip model. The results were generally very good in comparison with the experimental data. This would indicate that mechanical nonequilibrium is not an important factor in the flashing void development of initially subcooled flows. This conclusion seems reasonable in view of the fact that the velocities were generally quite high, corresponding to critical flow conditions, and relative velocities were generally quite low.

Specific conclusions include:

1. The bubble nucleation density and the resultant number density at the throat in nozzles with a subcooled inlet may vary by many orders of magnitude.
2. The throat void fraction is generally negligible in nozzles with subcooled inlets, even though the bubble number densities can be quite large.
3. The void development downstream of the throat is dependent on the size and number density of nuclei at flashing inception, these values being provided accurately by the new wall nucleation model for small geometries. Assumptions

of constant values for initial bubble size and/or number density, or any equivalent combination of assumptions for flashing inception, are incorrect.

4. Bulk nucleation has a negligible effect for small geometries.
5. Bulk nucleation becomes important for large geometries as the volume-to-surface ratio increases, but insufficient data exist to determine the transition factors.
6. The accuracy of the void calculations when compared with the existing data indicate that mechanical nonequilibrium is not an important factor in critical flow flashing of initially subcooled flows. Rather, thermal nonequilibrium, if accurately computed, is sufficient to provide adequate computation of global parameters.

REFERENCES

ABUAF, N., JONES, O. C. JR & WE, B. J. C. 1980 Critical flashing flow in nozzles with subcooled inlet conditions. In *Polyphase Flow and Transport Technology* (Edited by BAJURA, R. A.), pp. 65–74. ASME, New York.

ABUAF, N., ZIMMER, G. A. & WE, B. J. C. 1981 A study of nonequilibrium flashing of water in a converging–diverging nozzle, Vol. 1—Experimental. Reports NUREG/CR-1864 & BNL-NUREG-51317.

ABUAF, N., JONES, O. C., JR & WU, B. J. C. 1983 Critical flashing flow in nozzles with subcooled inlet conditions. *Trans. ASME Jl Heat Transfer* **105,** 379–383.

ARDRON, K. H. 1978 A two-fluid model for critical vapor–liquid flow. *Int. J. Multiphase Flow* **4,** 323–337.

ARDRON, K. H. & ACKERMAN, M. C. 1978 Studies of the critical flow of subcooled water in a pipe. In *Proc. 2nd CSNI Specialist Mtg*, Paris, pp. 517–543.

BAILEY, J. F. 1951 Metastable flow of saturated water. *Trans. ASME* **73,** 1109–1116.

BANKOFF, S. G. 1958 Entrapment of gas in the spreading of a liquid over a rough surface. *AIChE Jl* **4,** 24–26.

BEATTIE, D. R. H. 1973 A note on the calculation of two-phase pressure losses. *Nucl. Engng Des.* **25,** 395–402.

BROWN, R. A. 1961 Flashing expansion of water through a converging–diverging nozzle. M.S. Thesis, Univ. of California, Berkeley, CA. UKAEC Report UCRL-6665-T.

CELATA, C. P., CUMO, M., FARELLO, G. E. & INCALCATERRA, P. C. 1982 Critical flow of subcooled liquid and jet forces. Report ENEA-RT/INC(8218).

CHOW, H. & RANSOM, V. H. 1984 A simple interphase drag model for numerical two-fluid modeling of two-phase flow systems. In *2nd Proc. Nuclear Thermal Hydraulics, Summer A. ANS Mtg*, New Orleans, LA, pp. 137–145.

DOBRAN, F. 1985 A nonequilibrium model for the analysis of two-phase critical flows in tubes. Presented at the *23rd National Heat Transfer Conf.*, Denver, CO.

ELIAS, E. & CHAMBRE, P. L. 1984 A mechanistic non-equilibrium model for two-phase critical flow. *Int. J. Multiphase Flow* **10,** 21–40.

EPRI 1982 The Marviken full scale critical flow tests, Vol. 1. Summary Report. EPRI Report NP-2370.

EPRI 1983 Review and application of the TRAC-PD2 computer code. EPRI Report NP-2826.

ISHII, M. & MISHIMA, K. 1983 Flow regime transition criteria consistent with a two-fluid model for vertical two-phase flow. Reports NUREG/CR-3338 & ANL-83-42.

JONES, O. C. JR 1984 Thermal design concepts for the rotating fluidized bed reactor. *Nucl. Sci. Engng* **87,** 13–27.

JONES, O. C. JR & ZUBER, N. 1978 Bubble growth in variable pressure fields. *Trans. ASME Jl Heat Transfer* **100,** 453–459.

KARASEV, E. K., VASINGER, V. V., MINGALEYEVA, G. S. & TRUBKIN, E. I. 1977 Investigation of water adiabatic expansion from the saturation line. *Nucl. Energy* **42,** 478–481.

LASL 1979 TRAC-P1A. An advanced best-estimate computer program for PWR LOCA analysis. Reports NUREG/CR-0665 & LA-7777-MS.

LABUNTZOV, D. A., KOLCHUGIN, B. A., GOLOVIN, V. S., ZAKHAROVA, E. A. & VLADIMIROVA, L. N.

1964 High speed camera investigation of bubble growth for saturated water boiling in a wide range of pressure variations. *Thermophys. High Temp.* **2,** 446–453.

McFADDEN, J. H. *et al.* 1981 RETRAN-02. A program for transient thermal-hydraulic analysis of complex fluid flow systems. EPRI Report NP-1850 CCM, V.1.

NIGMATULIN, B. I. & SOPLENKOV, K. I. 1978 On the elementary theory of critical (maximum) two-phase mixture flow through variable-area channels. *Thermophys. High Temp.* **16,** 370–376.

RICHTER, H. J. & MINAS, S. E. 1981 Separated two-phase flow model: application to critical two-phase flow. EPRI Report NP-1800.

RIVARD, W. C. & TRAVIS, J. R. 1980 A nonequilibrium vapor production model for critical flow. *Nucl. Sci. Engng* **74,** 40–48.

SCHLICHTING, H. 1979 *Boundary Layer Theory.* McGraw Hill, New York.

SCRIVEN, L. E. 1959 On the dynamics of phase growth. *Chem. Engng Sci.* **1,** 1–13.

SHIN, T. S. & JONES, O. C. 1993 Nucleation and flashing in nozzles—1. A distributed nucleation model. *Int. J. Multiphase Flow* **19,** 943–964.

SKRIPOV, V. P. 1982 *Metastable Liquid,* pp. 255–265. Nauka, Moscow.

SOLBRIG, C. W., McFADDEN, J. H., LYCZKOWSKI, R. W. & HUGHES, E. D. 1978 Heat transfer and friction correlations required to describe steam–water behavior in nuclear safety studies. *AIChE Symp. Ser.* **74**(174), 100–128.

SOPLENKOV, K. I. & BLINKOV, V. N. 1983 Heterogeneous nucleation in the flow of superheated liquid. In *Multi-phase Systems: Transient Flows with Physical and Chemical Transformation* (Edited by NIGMATULIN, B. I. & IVANDAYEV, A. I.), pp. 105–109. Moscow State Univ.

SOZZI, G. L. & SUTHERLAND, W. A. 1975 Critical flow of saturated and subcooled water at high pressure. General Electric Report NEDO-13418.

WU, B. J. C., ABUAF, N. & SAHA, P. 1981 A study of nonequilibrium flashing of water in a converging–diverging nozzle, Vol. 2—Modeling. Reports NUREG/CR-1864 & BNL-NUREG-51317.